Addition of H_2 on (Sulfur, Phosphorus, Sulfur)-Pincer-Based Rhodium(I), Iridium(I), Palladium(II), and Platinum(II) Complexes: Reactivity and Regioselectivity

Marjolaine Doux, Louis Ricard, Pascal Le Floch,* and Yves Jean*

Laboratoire "Hétéroéléments et Coordination", UMR CNRS 7653, Département de Chimie, École polytechnique, 91128 Palaiseau Cédex, France

Received October 18, 2005

The addition of H_2 on (sulfur, phosphorus, sulfur)-pincer-based 16-VE complexes was studied from both experimental and theoretical points of view. The reaction of H_2 with [M(SPS)(PPh_3)] (M = Rh, Ir) led to the formation of dihydride M(III) complexes, which was fully characterized with iridium as metal. No reaction occurred with the isoelectronic 16-VE Pt(II) [Pt(SPS)Cl] complex. This reaction was also studied by means of DFT/B3PW91 calculations on the model complexes [M(SPS)(PH_3)] (M = Rh, Ir) and by B3PW91//ONIOM(B3PW91:UFF) calculations on real systems. The regioselectivity observed and the greater reactivity of the Ir compound were properly reproduced and related through a thermodynamic cycle to the electronic properties of the metal complex and to the energetics of the M−H bonds under formation. For both Rh and Ir complexes, the transition state for the formation of the dihydride product is a molecular dihydrogen complex located about 9 kcal mol^{-1} above the reactants. The reactivity of Pd(II) and Pt(II) analogues ([M(SPS)(X)], X = Cl, PH_3^+) was also studied, and the formation of M(IV) dihydrides was found to be much less favorable, especially for M = Pd. Non-oxidative-addition processes leading to molecular dihydrogen complexes or to an heterolytic cleavage of H_2 were also explored, but none of them were found to be favored on ΔG grounds.

Introduction

Since the pioneering work by Moulton and Shaw,[1] there has been a considerable and continuing interest in the synthesis and use of pincer ligands in coordination chemistry and catalysis.[2] This is largely due to their particular backbone that not only allows them to meridionally encapsulate transition metals but also permits a fine-tuning of their coordination behavior and their electronic properties. Recently, we reported on the synthesis and the coordination chemistry of SPS-based pincer ligands featuring two ancillary P═S ligands and a phosphorus atom as the central moiety.[3,4] Among these complexes, the 16-VE square-planar Rh(I) complex [Rh(SPS)(PPh_3)] (**1**) (Chart 1) proved to be particularly reactive toward small molecules such as O_2 and CS_2 and the corresponding 18-VE Rh(III) complexes [Rh(η^2-O_2)(SPS)(PPh_3)] and [Rh(η^2-CS_2)(SPS)(PPh_3)] were structurally characterized (Scheme 1).[5] Additionally, complex **1** also reacted with CO and SO_2 to yield the expected η^1-coordinated species. Later it was found that the iridium counterpart of **1**, [Ir(SPS)(PPh_3)] (**2**), could also activate O_2.[6]

Chart 1

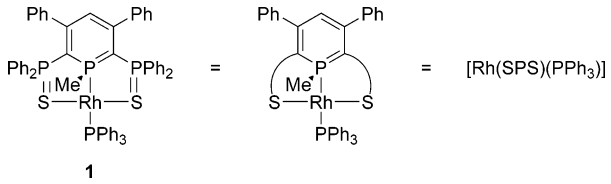

1

Scheme 1

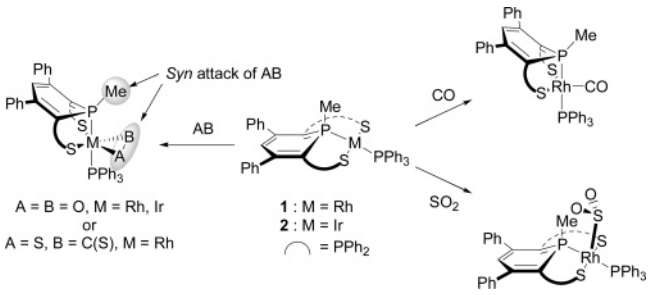

In all these cases, coordination of a new molecule occurred without ligand displacement and induced a complete change of the geometry of the complex from square planar (complexes **1** and **2**) to octahedral (for O_2 and CS_2), trigonal bipyramidal (for CO), or square pyramidal (for SO_2). Moreover, in all cases, the attack of the incoming ligand occurred regioselectively, the coordination taking place syn to the PMe moiety. This surprising planar discrimination was recently rationalized through DFT calculations in the case of O_2 and CO.[6,7]

The activation of dihydrogen by transition-metal complexes has been studied extensively for the two past decades and is of

* To whom correspondence should be addressed. E-mail: yves.jean@poly.polytechnique.fr (Y.J.); lefloch@poly.polytechnique.fr (P.L.F.)

(1) Moulton, C. J.; Shaw, B. L. *J. Chem. Soc., Dalton Trans.* **1976**, 1020−1024.

(2) (a) Albrecht, M.; Van Koten, G. *Angew. Chem., Int. Ed.* **2001**, *40*, 3750−3781. (b) van der Boom, M. E.; Milstein, D. *Chem. Rev.* **2003**, *103*, 1759−1792. (c) Singleton, J. T. *Tetrahedron Lett.* **2003**, *59*, 1837−1857.

(3) (a) Doux, M.; Mézailles, N.; Melaimi, M.; Ricard, L.; Le Floch, P. *Chem. Commun.* **2002**, 1566−1567. (b) Doux, M.; Ricard, L.; Le Floch, P.; Mézailles, N. *Dalton Trans.* **2004**, 2593−2600.

(4) Doux, M.; Mézailles, N.; Ricard, L.; Le Floch, P. *Eur. J. Inorg. Chem.* **2003**, 3878−3894.

(5) Doux, M.; Mézailles, N.; Ricard, L.; Le Floch, P. *Organometallics* **2003**, *22*, 4624−4626.

(6) Doux, M.; Ricard, L.; Le Floch, P.; Jean, Y. *Organometallics* **2005**, *24*, 1608−1613.

(7) Doux, M.; Le Floch, P.; Jean, Y. *J. Mol. Struct. (THEOCHEM)* **2005**, *724*, 73−79.

10.1021/om050900u CCC: $33.50
Publication on Web 01/31/2006

major importance in chemistry[8] and biology.[9] As part of our program on the activation of small molecules by square-planar SPS-based group 9 metal complexes, we recently explored the reactivity of complexes **1** and **2** toward H_2 from both an experimental and theoretical point of view. These results are presented herein, as well as a theoretical investigation on the reactivity of H_2 toward other d^8 metal complexes of group 10 metals featuring the same SPS ligand such as [M(SPS)X] (M = Pd, Pt, X = Cl, PH_3^+) complexes.

Experimental Results

The reactivity of complexes **1** and **2** toward H_2 was studied by bubbling dihydrogen (1 atm) at −78 °C into freshly prepared solution of the complexes. Both reactions resulted in a rapid color change of the solution from brown to orange. Significant changes were also observed in the ^{31}P NMR spectra of the crude mixtures (eq 1). For the rhodium complex **3**, a second-order

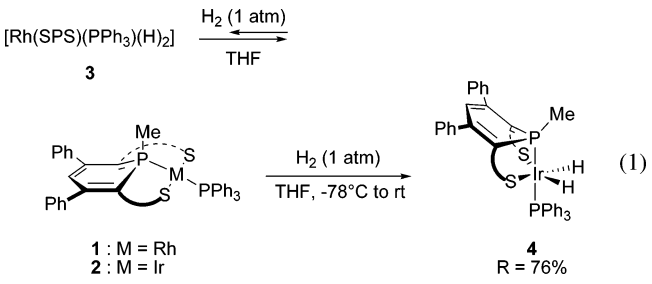

(1)

^{31}P NMR spectrum was observed which did not give structural information about the structure (AB_2C spin pattern with P_A = PMe, P_B = PPh_2, P_C = PPh_3). On the other hand, the AB_2Y spin system ^{31}P NMR spectrum of the iridium complex **4** indicated a symmetrical structure with two magnetically equivalent $Ph_2P_B(S)$ ancillary sidearms (δ(THF-d_8) 50.3 ppm, $^2J(P_B-P_A)$ = 107.0 Hz, and $^3J(P_B-P_Y)$ = 27.7 Hz with P_A = PMe, P_B = PPh_2, and P_Y = PPh_3). Moreover, the coupling constant $^2J(P_A-P_Y)$ of 336.0 Hz indicates a trans relation between the PMe and the PPh_3 moieties. The dihydride nature of complexes **3** and **4** was evidenced by ^1H NMR spectroscopy. In each spectrum, a characteristic chemical shift at −14.64 ppm for **3** and −18.39 ppm for **4** integrating for two protons was observed. The hydride signals appeared as a virtual triplet for **4** ($^2J(H-P_A)$ = $^2J(H-P_Y)$ = 15.5 Hz with P_A = PMe and P_Y = PPh_3) and as a doublet of virtual triplets for **3** ($^2J(H-P_A)$ = $^2J(H-P_C)$ = 12.3 Hz, $^1J(H-Rh)$ = 24.5 Hz with P_A = P-Me and P_C = PPh_3). Apart from the dihydride signals, the ^1H NMR spectra of complexes **3** and **4** are very similar. The stabilities of complexes **3** and **4** appeared to be very different. The solution containing the rhodium complex **3** evolved at room temperature under a N_2 atmosphere to yield back the square-planar complex **1** within several minutes, and despite many efforts, complex **3** could not be isolated or crystallized, evaporation of the solvent leading to the loss of the H_2 ligand. Therefore, complex **3** was only characterized by means of ^{31}P and ^1H NMR spectroscopy. The iridium complex **4** proved to be much more stable and was isolated and fully characterized by ^1H, ^{13}C, and ^{31}P spectroscopy and elemental analysis.

(8) (a) Kubas, G. J. *Metal Dihydrogen and Sigma-Bonded Complexes: Structure, Theory and Reactivity*, 1st ed.; Kluwer Academic/Plenum: London, 2001. (b) *Recent Advances in Hydride Chemistry*; Peruzzini, M. Poli, R., Eds.; Elsevier: Amsterdam, 2001. (c) Maseras, F.; Lledos, A.; Clot, E.; Eisenstein, O. *Chem. Rev.* **2000**, *100*, 601−636.

(9) Adams, M. W. W.; Stiefel, E. I. *Curr. Opin. Chem. Biol.* **2000**, *4*, 214−220.

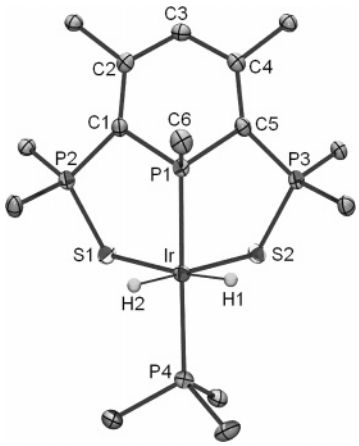

Figure 1. ORTEP view of complex **4**. Atoms are drawn as 50% thermal ellipsoids. The numbering is arbitrary and different from that used in NMR data. Selected bond lengths (Å) and angles (deg) are given in Table 3.

Table 1. Crystal Data and Structural Refinement Details for 4

formula	$C_{60}H_{51}IrP_4S_2 \cdot 2CH_2Cl_2$
M_r	1322.06
T (K)	150.0(1)
cryst syst	triclinic
space group	$P\bar{1}$
a (Å)	11.3410(10)
b (Å)	14.4510(10)
c (Å)	18.6570(10)
α (deg)	85.2690(10)
β (deg)	77.1100(10)
γ (deg)	73.9350(10)
V (Å^3)	2863.5(4)
Z	2
ρ (g cm^{-3})	1.533
μ (cm^{-1})	2.742
cryst size (mm)	0.21 × 0.20 × 0.12
F(000)	1328
index ranges	$-14 \le h \le 15$; $-20 \le k \le 20$; $-24 \le l \le 26$
$2\theta_{max}$ (deg)/criterion	30.03/$>2\sigma(I)$
no. of params refined; data/param	673; 21
no. of rflns collected	40 104
no. of indep rflns	16 646
no. of rflns used	14 664
wR2	0.0664
R1	0.0281
goodness of fit	1.018
largest diff peak/hole (e Å^{-3})	1.216 (0.115)/−1.185 (0.115)

On the basis of the extreme similarity between the ^1H NMR spectra of **3** and **4**, the same geometries for these complexes can be proposed with a high level of confidence. However, to fully ascertain the structure of the dihydride complex **3**, we attempted to get structural information from DFT calculations (vide supra).[8c] The formulation of **4** was definitively established through an X-ray crystal structure analysis. An ORTEP view of one molecule of **4** is presented in Figure 1, crystal data and structural refinement details are given in Table 1, and relevant bond distances and angles are listed in Table 3. As can be seen in Figure 1, complex **4** adopts an octahedral geometry (S1−Ir−S2 = 90.14(2)°, S1−Ir−H1 = 92.6(8)°, H1−Ir−H2 = 86(1)°). Interestingly, in this case again, the addition of H_2 occurs syn to the PMe moiety, as in O_2, CS_2, CO, and SO_2 complexes. As suggested by the ^1H NMR, an examination of the Ir−H (1.57(2) and 1.54(2) Å) and H−H distances (∼2.116 Å) revealed that **4** is an iridium(III) dihydride complex. Other

Scheme 2

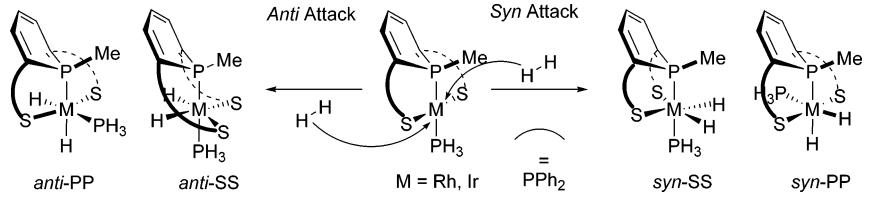

Table 2. Energy Decomposition (according to Scheme 3) for the Formation of the *syn*-SS (I), *anti*-PP (II), *syn*-PP (III), and *anti*-SS (IV) Dihydride Isomers by Addition of H_2 on the [M(SPS)(PH_3)] Complex[a]

(a) M = Rh				
	syn-SS (**Ia**)	*anti*-PP (**IIa**)	*syn*-PP (**IIIa**)	*anti*-SS (**IVa**)
$\Delta E_{dist}(ML_4)$	+27.5	+30.7	+32.1	+30.4
$\Delta E_{S/T}$	−4.0	−4.0	+1.4	+1.1
$\sum = \mathbf{\Delta E_{T,dist}}$	**+23.5**	**+26.8**	**+33.5**	**+31.5**
$-\Delta E_l(H-H)$	+107.3	+107.3	+107.3	+107.3
$2[\Delta E_l(M-H)]$	−144.8	−130.6	−132.1	−141.5
$\mathbf{\Delta E_R}$	**−14.0**	**+3.5**	**+8.7**	**−2.7**

(b) M = Ir				
	syn-SS (**Ib**)	*anti*-PP (**IIb**)	*syn*-PP (**IIIb**)	*anti*-SS (**IVb**)
$\Delta E_{dist}(ML_4)$	+36.4	+36.9	+40.8	38.9
$\Delta E_{S/T}$	−8.0	−1.2	+1.7	−3.2
$\sum = \mathbf{D E_{T,dist}}$	**+28.4**	**+35.7**	**+42.5**	**+35.7**
$-\Delta E_l(H-H)$	+107.3	+107.3	+107.3	+107.3
$2[\Delta E_l(M-H)]$	−170.9	−161.0	−162.7	−162.7
$\mathbf{\Delta E_R}$	**−35.2**	**−18.0**	**−12.9**	**−19.7**

[a] Energies are given in kcal mol^{-1}.

Table 3. Selected Theoretical Parameters Optimized for the Complex [Ir(SPS)(PR_3)($H)_2$] at the DFT-B3PW91 (R = H, Model Complex Ib) and ONIOM(B3PW91:UFF) (R = Ph, Real Complex Ib-rc) Levels of Calculation and Experimental Values for the Complex [Ir(SPS)(PPh_3)($H)_2$] (4)[a]

	DFT-B3PW91 (**Ib**, R = H)	ONIOM(B3PW91:UFF) (**Ib-rc**, R = Ph)	X-ray (**4**, R = Ph)
Ir−P1	2.289	2.272	2.2635(6)
Ir−P4	2.295	2.334	2.2920(6)
Ir−H1	1.583	1.583	1.57(2)
Ir−H2	1.583	1.585	1.54(2)
Ir−S1	2.558	2.526	2.4717(6)
Ir−S2	2.557	2.524	2.4514(5)
H1−H2	2.175	2.133	2.116
P1-Me	1.834	1.835	1.824(2)
P1−C2	1.795	1.802	1.785(2)
P1−C6	1.795	1.803	1.799(2)
P2−C2	1.761	1.784	1.771(2)
P3−C6	1.761	1.784	1.762(2)
P2−S1	2.017	2.022	2.0140(8)
P3−S2	2.017	2.024	2.0127(7)
C2−P1−C6	100.4	101.4	101.8(1)
∑(C−P1−C)	313.6	312.1	310.9
S1−Ir−S2	91.5	85.7	90.14(2)
P1−Ir−P4	173.2	171.0	176.70(2)
S1−Ir−H1	90.8	93.6	92.6(8)
H1−Ir−H2	86.8	84.7	86(1)
P1−C2−P2	111.7	101.0	111.7(1)
P1−C6−P3	111.7	101.5	111.3(1)

[a] Distances are given in Å and angles in deg. The numbering of atoms is shown in Figure 4.

geometricalparameters are quite similar to those for other SPS-based group 9 complexes.[5,6]

Similar experiments were carried out with the isoelectronic Pt(II) complex **5** (eq 2), but no other compound than the starting material could be observed even when a high pressure of H_2 was used (note that no NMR experiments under pressure have been carried out).

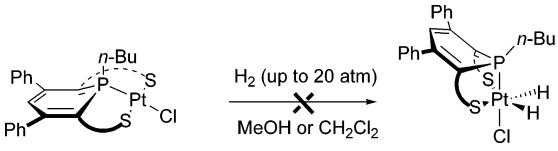

5 (2)

Theoretical Approach

The addition of H_2 on the SPS-type pincer-based Rh(I), Ir-(I), Pd(II), and Pt(II) complexes was studied by means of DFT calculations. Four modes of attack were considered (*syn*-SS, *anti*-SS, *syn*-PP, and *anti*-PP) for the cis addition of H_2, depending whether the incoming H_2 molecule is located (i) syn or anti to the P−Me bond and (ii) coplanar to the M−S bonds (SS) or to the M−P bonds (PP) (Scheme 2).

Group 9 (M = Rh, Ir). Calculations were performed on the model complexes (quoted as [M(SPS)(PH_3)]), in which all phenyl groups were replaced by H atoms, and on the real complexes (quoted as [M(SPS)(PPh_3)]). The regioselectivity of the addition and the influence of the nature of the metal center on both the transition state energy and the exothermicity of the addition reaction are related through a thermodynamic cycle to the electronic properties of the metal complex and to the energies of the M−H bonds formed.

Different geometries of the [Rh(SPS)(PH_3)($H)_2$] complexes were optimized by considering four modes of attack, as defined in Scheme 2. In each case a minimum-energy structure was characterized. In agreement with the planar discrimination reported previously for this complex, the *syn*-SS isomer was found to be the most stable, the energy ordering being as follows (in kcal mol^{-1}): *syn*-SS (0) (**Ia**) < *anti*-SS (+11.3) (**IVa**) < *anti*-PP (+17.5) (**IIa**) < *syn*-PP (+22.7) (**IIIa**). Furthermore, the *syn*-SS isomer is the only isomer which is significantly more stable than the isolated reactants (ΔE_R = −14.0 kcal mol^{-1}). The structures of the four minima (**Ia**−**IVa**) are given in Figure 2, together with selected geometrical parameters. In the four isomers, both the H···H and the Rh−H distances are consistent with a *cis*-dihydride structure (in the most stable *syn*-SS isomer (**Ia**) H···H = 2.085 Å and Rh−H = 1.550 Å). The *syn*-SS (**Ia**), *anti*-PP (**IIa**), and *syn*-PP (**IIIa**) isomers can be described as Rh(III) octahedral complexes, while the *anti*-SS attack induced the decoordination of a sulfur ligand, leading to a Rh(III) center in a distorted square base pyramidal environment with a hydride at the apical position (**IVa**).

The electronic factors responsible for the regioselectivity of the cis oxidative addition of H_2 can be analyzed by means of a thermodynamic cycle which connects the separate reactants (^{1}[Rh(SPS)(PH_3)] + H_2) to the dihydride species (Scheme 3). The reaction is decomposed in the following steps: (i) distortion of the ^{1}[Rh(SPS)(PH_3)] complex from its equilibrium geometry to its geometry in the product ($\Delta E_{dist}(ML_4)$); (ii) formation of the triplet state of this distorted metal fragment ($\Delta E_{S/T}$) with

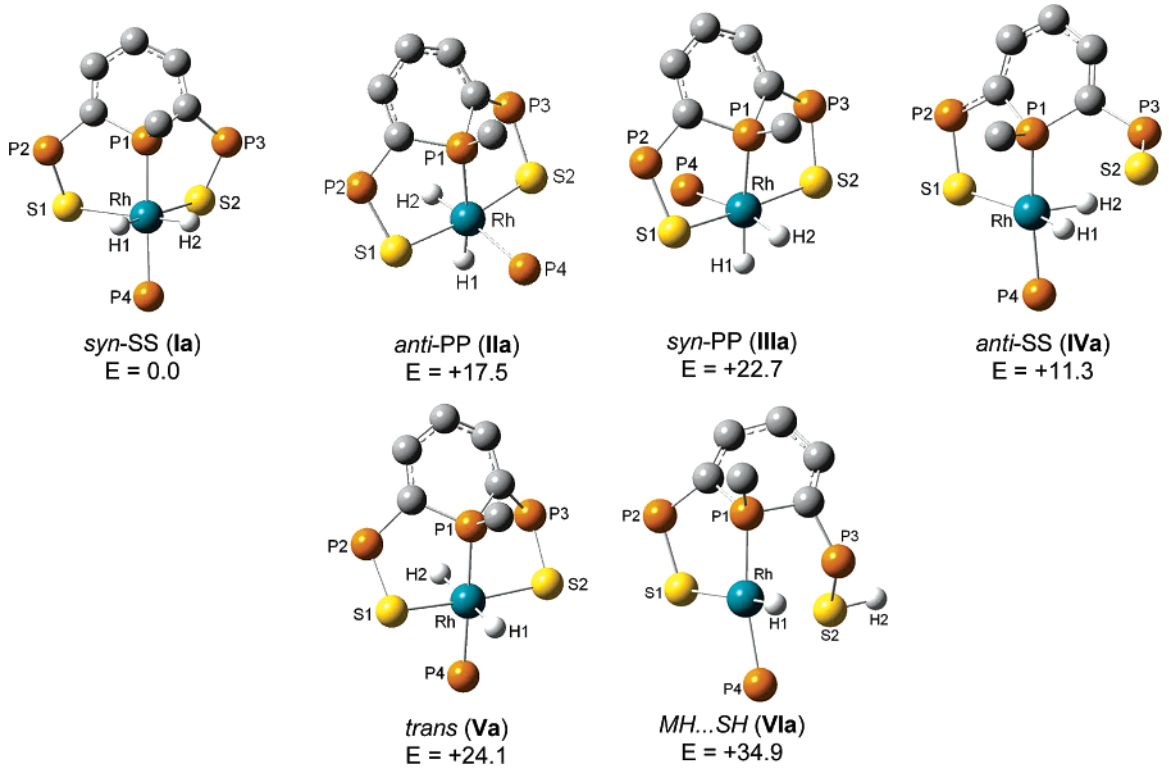

Figure 2. Optimized geometries of unsubstituted rhodium complexes **Ia**−**VIa**. Hydrogen atoms are omitted for clarity, except for those bound to the metal center. Selected geometrical parameters (bond distances in Å and angles in deg) are as follows. **Ia**: Rh−H = 1.550; S1−Rh−S2 = 93.9, P1−Rh−P4 = 171.3. **IIa**: Rh−H1 = 1.574, Rh−H2 = 1.565; S1−Rh−S2 = 172.2, P1−Rh−P4 = 101.7. **IIIa**: Rh−H1 = 1.603, Rh−H2 = 1.554; S1−Rh−S2 = 172.0, P1−Rh−P4 = 106.2. **IVa**: Rh−H1 = 1.510, Rh−H2 = 1.547, Rh−S1 = 2.480, Rh−S2 = 4.736; S1−Rh−H2 = 124.6, S1−Rh−H1 = 165.3, P1−Rh−P4 = 172.1. **Va:** Rh−H1 = 1.638, Rh−H2 = 1.684, Rh−S1 = 2.426, Rh−S2 = 2.426. **VIa**: Rh−H1 = 1.562, S2−H2 = 1.358, Rh−S1 = 2.530, Rh−S2 = 3.252; S1−Rh−H1 = 168.0. *E* is the relative energy, given in kcal mol^{-1}.

Scheme 3

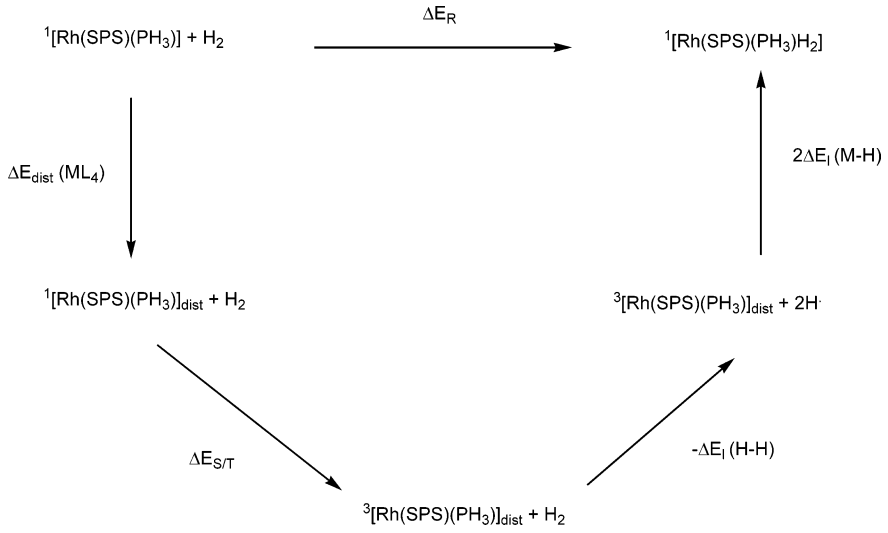

two unpaired electrons (the metal fragment is now in the optimal situation to bind two additional ligands); (iii) breaking of the H−H bond ($-\Delta E_l(H_2)$); (iv) formation of the two Rh−H bonds ($2[\Delta E_l(M-H)]$).[6,7,10] The energy variation associated with the addition reaction can thus be expressed as $\Delta E_R = \Delta E_{dist}(ML_4) + \Delta E_{S/T} - \Delta E_l(H-H) + 2[\Delta E_l(M-H)]$. In the following discussion, the first two terms will be most often considered together, since their sum (quoted as $\sum = \Delta E_{T,dist}$) represents the energy required to "prepare" the metal fragment for the oxidative addition reaction. This energy decomposition scheme clearly shows that the addition process of H_2 is favored by a low $\Delta E_{T,dist}$ value and a large M−H bonding energy.

The results of this energy decomposition are given in Table 2a. As has been shown previously,[6,7,10] the triplet state energy of a metal fragment turns out to be an important factor in predicting its reactivity for an oxidative addition reaction. As a matter of fact, the most stable isomer (*syn*-SS, **Ia**) has the

(10) (a) Lesnard, H.; Demachy, I.; Jean, Y.; Lledos, A. *Chem. Commun.* **2003**, 850−851. (b) Tomas, J.; Lledos, A.; Jean, Y. *Organometallics* **1998**, *17*, 4932−4939. (c) Su, M.-D.; Chu, S.-Y. *J. Am. Chem. Soc.* **1997**, *119*, 5373−5383.

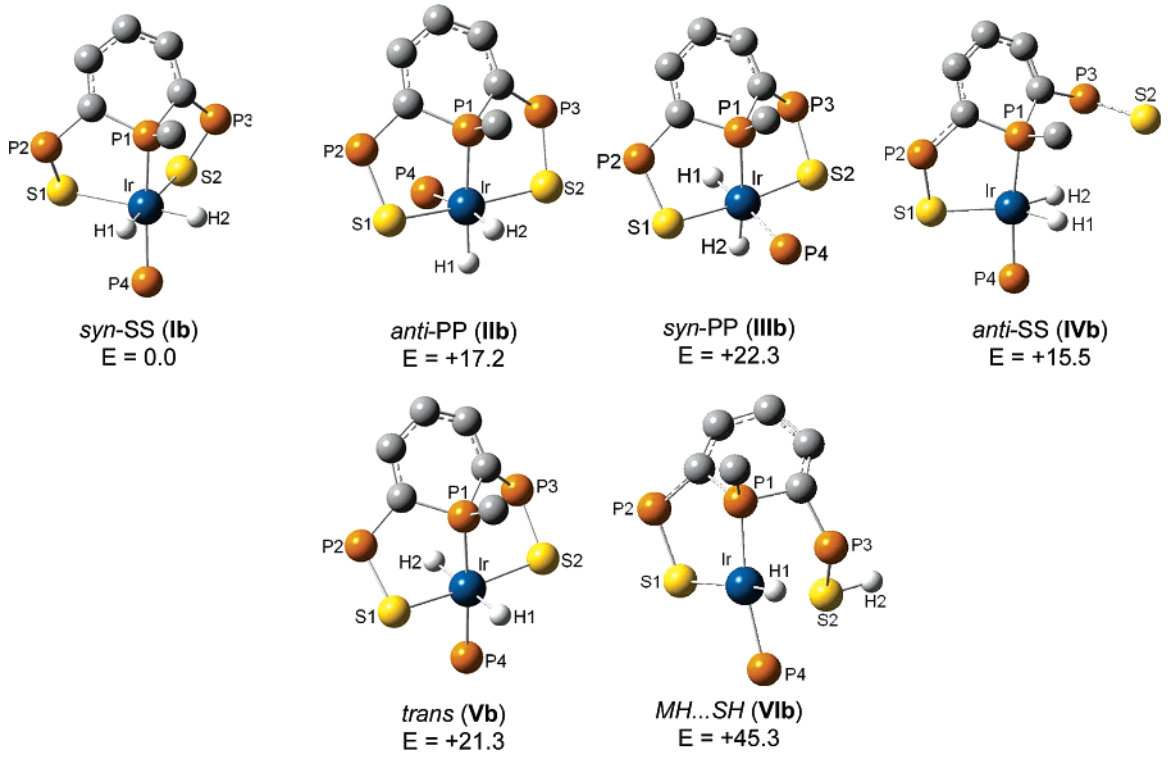

Figure 3. Optimized geometries of unsubstituted iridium complexes **Ib**−**VIb**. Hydrogen atoms are omitted for clarity, except for those bound to the metal center. Selected geometrical parameters (bond distances in Å and angles in deg) are as follows. **Ib**: Ir−H = 1.583; S1−Ir−S2 = 91.5, P1−Ir−P4 = 171.2. **IIb**: Ir−H1 = 1.611, Ir−H2 = 1.607; S1−Ir−S2 = 173.0, P1−Ir−H1 = 168.9, P4−Ir−H2 = 171.6. **IIIb**: Ir−H1 = 1.632, Ir−H2 = 1.596; S1−Ir−S2 = 172.5, P1−Ir−P4 = 106.0, P1−Ir−H1 = 172.1. **IVb**: Ir−H1 = 1.551, Ir−H2 = 1.567, Ir−S1 = 2.410, Ir−S2 = 4.735; S1−Ir−H1 = 137.5, S1−Ir−H2 = 152.6, P1−Ir−P4 = 1723.0. **Vb**: Ir−H1 = 1.650, Ir−H2 = 1.696; H1−Ir−H2 = 180.0. **VIb**: Ir−H1 = 1.588, S2−H2 = 1.356, Ir−S1 = 2.475, Ir−S2 = 3.260; S1−Ir−H1 = 166.3. *E* is the relative energy, given in kcal mol^{-1}.

smallest $\Delta E_{T,dist}$ value.[11] Furthermore, formation of this isomer is also favored by the largest Rh−H bond energy. The planar discrimination between the *syn*-SS and *anti*-SS attacks ($\Delta(\Delta E_R)$ = 11.3 kcal mol^{-1} in favor of the former) and between the *syn*-PP and *anti*-PP isomers ($\Delta(\Delta E_R)$ = 5.2 kcal mol^{-1} in favor of the latter) can be mainly traced to the triplet state energy of the metal fragment: $\Delta(\Delta E_{T,dist})$ = +8.0 kcal mol^{-1} for the SS isomers and +6.7 kcal mol^{-1} for the PP isomers.

Although the *syn*-SS isomer was found to be more stable than the isolated reactants by 14.0 kcal mol^{-1}, it must be noted that the entropy term does not favor this addition process. The computed ΔG value is actually close to zero (ΔG_R = −2.2 kcal mol^{-1}), a result which is in agreement with the reversibility of the addition observed in solution. Note that the *cis*−*trans* isomerization is not expected to occur in the dihydride complex, the energy of the isomer with the hydrides *trans* to each other (Figure 2, **Va**) being located 24.1 kcal mol^{-1} above that of the *cis* (*syn*-SS) isomer (**Ia**).[12,13] Finally, a second pathway has been envisioned for the activation of dihydrogen by the square-planar Rh(I) complex [Rh(SPS)(PH_3)]. The complex resulting from an heterolytic activation of H_2 (H^- attacking the metal center and H^+ reacting with a lone pair of a decoordinated S ancillary ligand) has been studied.[14] Heterolytic activation is classical for metal sulfide compounds.[15] The resulting nearly square-planar Rh(I) complex (quoted as [Rh(H)(SP···SH)(PH_3)]) (Figure 2, **VIa**) was found to be located 34.9 kcal mol^{-1} above **Ia**, so that its formation can be excluded on energetics grounds. Note that our attempts to find a stable molecular dihydrogen complex failed, the starting complexes evolving toward a previously optimized dihydride structure.

Similar calculations were performed on the Ir counterpart. The same energy ordering was found for the four isomers depicted in Scheme 2 (kcal mol^{-1}): *syn*-SS (0) (**Ib**) < *anti*-SS (+15.5) (**IVb**) < *anti*-PP (+17.2) (**IIb**) < *syn*-PP (+22.3) (**IIIb**). Structures of the four minima (**Ib-IVb**) are presented in Figure 3 together with selected geometrical parameters. The lowest energy structure (*syn*-SS, **Ib**) is in agreement with the experimental structure (Figure 1), and the main geometrical parameters are satisfactorily reproduced (Table 3): Ir−H = 1.583 Å (exptl 1.55(2) Å average), Ir−P1 = 2.289 Å (exptl 2.2635(6) Å), Ir−P4 = 2.295 Å (exptl 2.2920(6) Å), Ir−S1 = 2.558 Å (exptl 2.4717(6) Å), Ir−S2 = 2.557 Å (exptl 2.4514-(6) Å). The structures of the three other isomers resemble those

(11) The triplet state is found to be more stable than the singlet state in some of the distorted metal fragments. This result should be considered with some caution, since DFT calculations are often considered to overstabilize the high spin states.

(12) The addition of H_2 on Vaska's complexes also leads to octahedral complexes with cis dihydrides.

(13) Deutsch, P. P.; Eisenberg, R. *Chem. Rev.* **1988**, *88*, 1147−1161.

(14) (a) Gruet, K.; Clot, E.; Eisenstein, O.; Lee, D. H.; Patel, B.; Macchioni, A.; Crabtree, R. H. *New J. Chem.* **2003**, *27*, 80−87. (b) Lee, D. H.; Patel, B. P.; Clot, E.; Eisenstein, O.; Crabtree, R. H. *Chem. Commun.* **1999**, 297−298. (c) Collman, J. P. *Nat. Struct. Biol.* **1996**, *3*, 213-217. (d) Collman, J. P.; Hegedus, L. S.; Norton, J. R.; Finke, R. G. *Principles and Applications of Organotransition Metal Chemistry*; University Science Books: Mill Valley, CA, 1987. (e) Clapham, S. E.; Hadzovic, A.; Morris, R. H. *Coord. Chem. Rev.* **2004**, *248*, 2201−2237. (f) Abdur-Rashid, K.; Clapham, S. E.; Hadzovic, A.; Harvey, J. N.; Lough, A. J.; Morris, R. H. *J. Am. Chem. Soc.* **2002**, *124*, 15104−15118.

(15) (a) Linck, R. C.; Pafford, R. J.; Rauchfuss, T. B. *J. Am. Chem. Soc.* **2001**, *123*, 8856−8857. (b) Ienco, A.; Calhorda, M. J.; Reinhold: J.; Reineri, F.; Bianchini, C.; Peruzzini, M.; Vizza, F.; Mealli, C. *J. Am. Chem. Soc.* **2004**, *126*, 11954−11965. (c) Sellmann, D.; Prakash, R.; Heinemann, F. W.; Moll, M.; Klimowicz, M. *Angew. Chem., Int. Ed.* **2004**, *43*, 1877−1880.

described above for the Rh analogue. The energy decomposition, according to the thermodynamic cycle given in Scheme 3, also reveals similar trends (Table 2b). In particular, the formation of the *syn*-SS isomer is favored both by the lowest value for $\Delta E_{T,dist}$ and by the largest Ir−H bond energy.[16] No *cis*−*trans* isomerization is expected to occur in the *syn*-SS isomer, since the *trans* isomer (**Vb**) was located 21.3 kcal mol^{-1} higher in energy. Finally, the nearly square-planar monohydride complex [Ir(H)(SP···SH)(PH_3)] (**VIb**), resulting from an heterolytic activation of H_2, was also studied. It was found to be 45.3 kcal mol^{-1} higher in energy than **Ib**; thus, its formation can be excluded.

The major change on going from the Rh to the Ir complex is the large increase of the exothermicity of the addition reaction, from −14.0 to −35.2 kcal mol^{-1}. The use of the thermodynamic cycle described in Scheme 3 offers a simple explanation for this result. Comparison of the energy decomposition for the Rh (**Ia**) and Ir (**Ib**) *syn*-SS isomers (Table 2) shows that the energetic term associated with the distortion of the metal fragment ($\Delta E_{T,dist}$) works in favor of the Rh complex, by 4.9 kcal mol^{-1}. The factor which makes the reaction with the Ir complex more exothermic is the M−H bonding energy, which is larger for Ir (−85.45 kcal mol^{-1} per bond) than for Rh (−72.4 kcal mol^{-1} per bond).[17] This result exemplifies another important factor in predicting the reactivity of a complex for an oxidative addition reaction: the energetics of the metal−ligand bonds under formation. The larger exothermicity found for the iridium complex nicely rationalizes the different behavior of two complexes with respect to the addition of H_2. As a matter of fact, ΔG_R is now largely negative (−22.2 kcal mol^{-1} for Ir instead of −2.2 kcal mol^{-1} for Rh), in agreement with the experimental observation of an irreversible formation of a dihydride upon H_2 addition on the Ir complex.

To evaluate the influence of the phenyl substituents located on the central heterocycle and the triphenylphosphine ligands, additional calculations were performed on the real complexes (**rc**) at the B3PW91//B3PW91:UFF level. The geometry of the reactant [M(SPS)(PPh_3)] (M = Rh, Ir) and the *syn*-SS species [M(SPS)(PPh_3)(H_2)] (**Ia-rc**, M = Rh; **Ib-rc**, M = Ir) were optimized. The main theoretical parameters of the Ir compound **Ib-rc** (Figure 4) are reported in Table 3 for sake of comparison with the theoretical parameters of the unsubstituted complex and with experimental values.

From an energetic point of view, the exothermicity of the addition reaction increases by 21.2 kcal mol^{-1} on going from Rh to Ir (Table 4); the same value was found for the unsubstituted model complexes. The thermodynamic cycle depicted in Scheme 3 was recalculated with the real complexes. The energy decomposition given in Table 4 clearly shows that

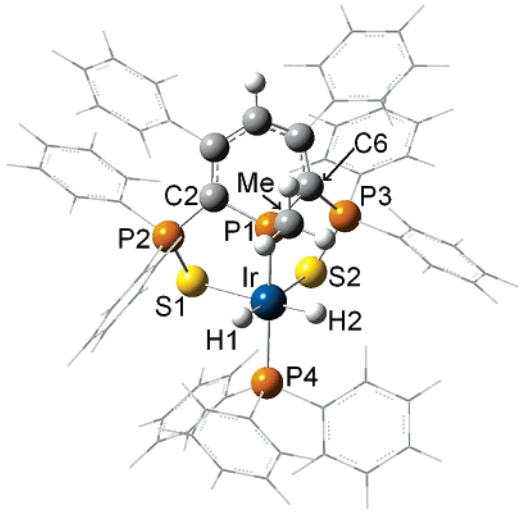

Figure 4. Optimized structure of the complex [Ir(SPS)(PPh_3)(H_2)] (**Ib-rc**) at the ONIOM (B3PW91:UFF) level of calculation. Atoms included in the QM part are shown in ball-and-stick format, and atoms included in the MM part are represented by tubes.

Table 4. Energy Decomposition (According to Scheme 3) for the Formation of the *syn*-SS Complexes by Addition of H_2 on the Model Complexes [M(SPS)(PH_3)] (M = Rh (Ia), Ir (Ib)) and on the Real Complexes [M(SPS)(PPh_3)] (M = Rh (Ia-rc), Ir (Ib-rc))[a]

	Rh (**Ia**)	Rh (**Ia-rc**)	Ir (**Ib**)	Ir (**Ib-rc**)
$\Delta E_{dist}(ML_4)$	+27.5	+21.1	+36.4	+30.3
$\Delta E_{S/T}$	−4.0	−4.2	−8.0	−9.1
$\Sigma = \mathbf{\Delta E_{T,dist}}$	**+23.5**	**+16.9**	**+28.4**	**+21.2**
$-\Delta E_l$(H−H)	+107.3	+107.3	+107.3	+107.3
2[ΔE_l(M−H)]	−144.8	−144.7	−170.9	−170.2
$\mathbf{\Delta E_R}$	**−14.0**	**−20.5**	**−35.2**	**−41.7**

[a] Energies are given in kcal mol^{-1}.

the M−H bonding energy is still responsible for the change in the reaction energy ΔE_R. Note that the ΔE_l(M−H) bond energies computed for the real complexes are close to those found for the unsubstituted models (−85.1 kcal mol^{-1} (Ir) and −72.35 kcal mol^{-1} (Rh) instead of −85.45 and −72.4 kcal mol^{-1}, respectively).[17]

Finally, the mechanism for the addition of H_2 to the [M(SPS)(PH_3)] complexes was elucidated by the optimization and the characterization of the transition state structure leading to the most stable *syn*-SS isomer (Figure 5). For both of them (**TS-Ia**, M = Rh; **TS-Ib**, M = Ir), the H−H bond is only slightly elongated (0.818 and 0.825 Å for **TS-Ia** and **TS-Ib**, respectively) with respect to its value in the isolated H_2 molecule (0.744 Å), and the M−H distances are 0.3−0.4 Å longer than in the dihydride product. On the other hand, the metal fragment is distorted from its initial square-planar geometry, with S−M−S angles of 139.6° (M = Rh, **TS-Ia**) and 153.3° (M = Ir, **TS-Ib**). Therefore, the transition state can be described as a five-coordinated Rh(I) or Ir(I) complex in a distorted-trigonal-bipyramidal geometry, with a molecular dihydrogen as an equatorial ligand. Such a slight H−H bond lengthening in the transition state has been already found for the H_2 oxidative addition to Vaska's complexes.[13] According to the values optimized for the bending of the M−S bonds, the transition state for the Ir complex, **TS-Ib,** is found to be "earlier" than that for the Rh complex, in agreement with the greater exothermicity of the addition reaction found for the iridium compound. In that respect, the trend found for the activation energies ($\Delta E^{\ddagger}$) is rather unexpected, since it is found to be slightly higher for Ir, **TS-Ib** (+9.2 kcal mol^{-1}), than for Rh,

(16) In the isomers which adopt a similar pseudo-octahedral geometry within a given metal, the M−H bond energy is significantly larger for M−H *trans* to M−S (*syn*-SS isomer) than for M−H *trans* to M−P (*syn*-PP and *anti*-PP isomers). This result may be traced to the weaker *trans* influence exerted by the sulfur ligand.

(17) (a) Martinho Simoes, J. A.; Beauchamp, J. L. *Chem. Rev.* **1990**, *90*, 629−688. (b) In our thermodynamic cycle, the M−H bond energy is defined with respect to the distorted (or nonreoganized) metal fragment. Another possibility is to define this term with respect to the metal fragment in its optimized geometry. In that case, the distortion energy does not appear explicitly in the thermodynamic cycle but is included in the bond energy term. The absolute values of M−H bond energy depend on this choice, but the general trend (increase of the bond energy in going from Rh to Ir) remains: E_l(Rh−H) = −60.7 kcal mol^{-1} instead of −71.3 kcal mol^{-1} and E_l(Ir−H) = −72.4 kcal mol^{-1} instead of −85.5 kcal mol^{-1}. Note that the lower values are in good agreement with experimental data for Rh (61.8 ± 5 kcal mol^{-1}) and Ir (−74.0 ± 5 kcal mol^{-11}) complexes, which are derived from the thermodynamic cycle in which the metal fragment is taken in its ground-state geometry.

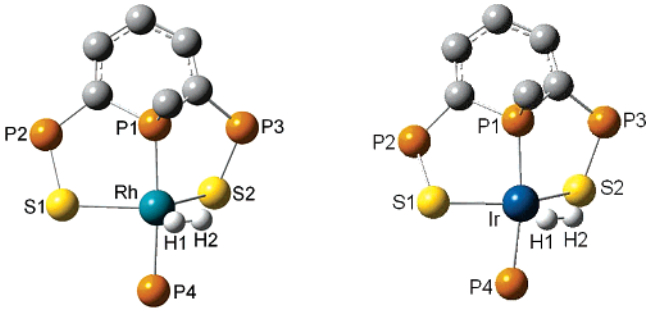

Figure 5. Optimized geometries of the transition states for the addition of H_2 on the unsubstituted rhodium and iridium complexes (**TS-Ia** and **TS-Ib**, respectively). Hydrogen atoms are omitted for clarity, except for those bound to the metal center. Selected geometrical parameters (bond distances in Å and angles in deg) are as follows. Rh (**TS-Ia**): H−H = 0.818, Rh−H (av) = 1.886; S−Rh−S = 131.6, P1−Rh−P4 = 170.7. Ir (**TS-Ib**): H−H = 0.825, Ir−H (av) = 1.921; S−Ir−S = 153.3, P1−Ir−P4 = 162.3.

Table 5. Energy Decomposition (According to Scheme 4) of the Activation Energy ($\Delta E^{\ddagger}$) for the Addition of H_2 Leading to the *syn*-SS Dihydride (M = Rh (TS-Ia), Ir (TS-Ib))[a]

	Rh (**TS-Ia**)	Ir (**TS-Ib**)
$\Delta E_{S,dist}$	+9.8	+7.8
$\Delta E_{stretch}$(H−H)	+2.0	+2.4
ΔE_{int}	−3.2	−1.0
$\Delta E^{\ddagger}$	**+8.6**	**+9.2**

[a] Energies are given in kcal mol^{-1}.

TS-Ia (+8.6 kcal mol^{-1}). The same holds for the $\Delta G^{\ddagger}$ values (19.1 and 19.6 kcal mol^{-1} for M = Rh, Ir, respectively). These values are fully consistent with a reaction experimentally conducted at −78 °C.

This result was analyzed by means of a thermodynamic cycle in which, according to the results given above, the transition state is described as a slightly elongated molecular dihydrogen molecule in interaction with the distorted [M(SPS)(PH$_3$)] metal fragment in its *singlet state* (Scheme 4). The activation energy ($\Delta E^{\ddagger}$) is thus equal to the sum of (i) the distortion energy of the metal fragment in its singlet state (ΔE_{dist}(ML$_4$)), (ii) the stretching energy of H_2 ($\Delta E_{stretch}$(H−H)), and (iii) the interaction energy of the two fragments (ΔE_{int}).

The computed ΔE_{dist}(ML$_4$) term, which represents most of the activation energy (Table 5), is actually smaller for the Ir metal fragment, which is less distorted than its Rh analogue (+7.8 kcal mol^{-1} instead of +9.8 kcal mol^{-1}). The interaction energy term (ΔE_{int}) found to be more favorable for M = Rh (−3.2 kcal mol^{-1}) than for M = Ir (−1.0 kcal mol^{-1}) is thus responsible for the slight increase of the activation energy in going from M = Rh to M = Ir.

Note that the barrier for the reverse reaction (*syn*-SS dihydride → TS) increases from 22.6 kcal mol^{-1} (Rh) to 44.4 kcal mol^{-1} (Ir). This result can be analyzed by a thermodynamic cycle, similar to that of Scheme 3, which connects the dihydride complexes (**Ia** or **Ib**) to the transition state complexes (**TS-Ia** or **TS-Ib**). The step mainly responsible for this trend involves the breaking of two M−H bonds (+144.8 and +170.9 kcal mol^{-1} for Rh and Ir, respectively (see Table 2)).

It is noteworthy that, in both transition states, the interaction energy between the two fragments is very small, despite rather short M−H distances (1.887 Å (av) for Rh and 1.920 Å (av) for Ir). This striking result can be qualitatively rationalized by analyzing the main molecular orbital interactions at work in the transition state (Scheme 5): The σ_{H_2} MO interacts mainly

Scheme 5. Main Orbital Interactions between H_2 and the Metal Fragment in the Transition State Structures TS-Ia and TS-Ib

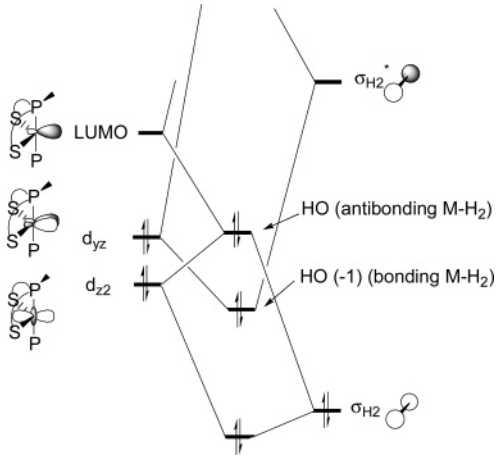

with the occupied d_{z^2} orbital and, to a lesser extent, with the LUMO of the d^8 metal fragment in a butterfly geometry. On the other hand, σ_{H_2}* interacts with the occupied nonbonding d_{yz} orbital. The important point is that a destabilizing four-electron interaction (σ_{H_2} ↔ d_{z^2}) adds to the two stabilizing two-electron interactions (σ_{H_2} ↔ LUMO donation and d_{yz} ↔ σ_{H_2}* back-donation interactions). The existence of this repulsive interaction leads to an antibonding M−H_2 character of the HO in the transition state and gives a qualitative understanding of the nearly zero total interaction energy computed between the metal and dihydrogen fragments.

This qualitative analysis is confirmed by the shape of the two highest occupied MOs pictured in Figure 6: the HOMO-1 is bonding between M and H_2 and characterizes the back-donation interaction (d_{yz} ↔ σ_{H_2}*), while the HOMO is antibonding between M and H_2 (d_{z^2}(polarized) ↔ σ_{H_2}).

Scheme 4

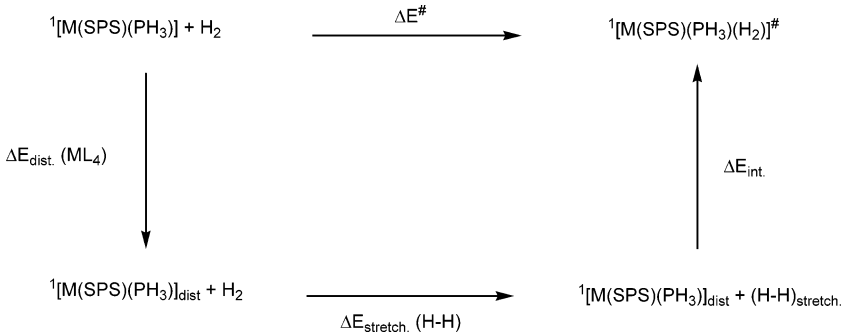

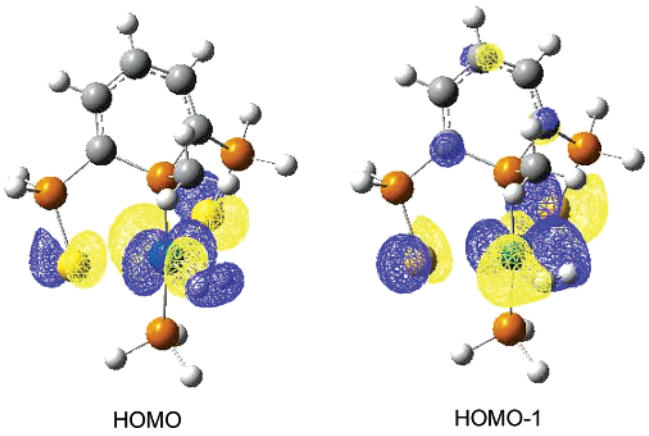

Figure 6. Drawing of the two highest occupied MOs in the transition state structure **TS-Ia** for the addition of H_2 on the [Rh(SPS)(PH_3)] complex.

In conclusion, the regioselectivity of the addition of H_2 to the [Ir(SPS)(PH_3)] complex is well reproduced by DFT calculations and a similar structure is predicted for the Rh analogue. The planar discrimination in favor of the *syn*-SS isomer is governed by a metal fragment property, i.e. the energy required to form the distorted complex in its lowest triplet state, and by the strength of the M−H bonds under formation. On the other hand, the increase of the exothermicity of the reaction on going from Rh to Ir is traced by the increase of the M−H bonding energy. Finally, the transition state structure for this oxidative addition reaction is depicted as a molecular dihydrogen complex located only 8−9 kcal mol^{-1} above the reactants.

Group 10 (M = Pd, Pt). The addition of H_2 was studied on the SPS-type pincer-based Pd(II) and Pt(II) unsubstituted model complexes [M(SPS)(X)] (X = Cl, $(PH_3)^+$). Among the various dihydride structures optimized and characterized as minima, the *syn*-SS isomer was always found to be the most stable (**Ic**−**f**, Figure 7). The addition reaction was found to be much easier for M = Pt (ΔE_R = −0.3 and +1.2 kcal mol^{-1} for X = Cl and $(PH_3)^+$, respectively) than for M = Pd (+22.3 and +24.6 kcal mol^{-1} for X = Cl and $(PH_3)^+$, respectively).

As was found for group 9 complexes, the M−H bonding energy increases on going from the second to the third transition metal series (61.4 and 74.8 kcal mol^{-1} per bond for Pd and Pt, respectively (mean values)). However, in marked contrast with the group 9 metal complexes, for which the addition of H_2 was found to be very exothermic, the computed reaction energy (ΔE_R) is either close to zero (Pt) or largely positive (Pd).

Table 6. Energy Decomposition (According to Scheme 3) for the Formation of the *syn*-SS Complexes by Addition of H_2 on the Complexes [Pd(SPS)(X)] (X = Cl (Ic), $(PH_3)^+$ (Id)) and [Pt(SPS)(X)] (X = Cl (Ie), $(PH_3)^+$ (If))[a]

	PdCl (**Ic**)	$PdPH_3^+$ (**Id**)	PtCl (**Ie**)	$PtPH_3^+$ (**If**)
$\Delta E_{dist}(ML_4)$	25.0	+32.2	+35.0	+40.1
$\Delta E_{S/T}$	+9.8	+11.0	+4.9	+5.5
$\sum = \mathbf{\Delta E_{T,dist}}$	**+34.8**	**+43.2**	**+39.9**	**+45.6**
$-\Delta E_I$(H−H)	107.3	107.3	107.3	107.3
2[ΔE_I(M−H)]	−119.8	−125.9	−147.5	−151.7
$\mathbf{\Delta E_R}$	**+22.3**	**+24.6**	**−0.3**	**+1.2**

[a] Energies are given in kcal mol^{-1}.

Moreover, the ΔG_R values are now positive for the four complexes (+33.7, +36.5, +11.5, and +13.4 kcal mol^{-1} for **Ic**−**f**, respectively), in agreement with the experimental observation. As a matter of fact, the addition of H_2 on [Pt(SPS)(Cl)] (**5**) has been carried out in MeOH and CH_2Cl_2 at 20 bar and no reaction occurred. These results reflect the difficulty of forming a group 10 M(IV) complex, in particular in the Pd case, compared to the formation of Rh(III) or Ir(III) complexes. The energetic decompositions given in Table 2 (M = Rh (**Ia**) and M = Ir (**Ib**)) and Table 6 (M = Pd (**Ic**,**d**)) and M = Pt (**Ie**,**f**)) allow us to trace the electronic factors responsible for such a change. Let us first note that the energy required to distort the reactant in its singlet state (ΔE_{dist}) is similar for Rh and Pd complexes (27.5 (av) and 28.6 (av) kcal mol^{-1}, respectively) and for Ir and Pt (36.4 (av) and 37.6 (av) kcal mol^{-1}, respectively). *Two factors* were found to work against the reactivity of group 10 metal complexes: (i) the singlet/triplet energy separation in the distorted reactant ($\Delta E_{S/T}$ for the *syn*-SS isomer), which is found to be larger by 13−15 kcal mol^{-1}; (ii) the energy gain associated with the formation of the two M−H bonds, decreasing by about 22 kcal mol^{-1} on going from Rh to Pd or from Ir to Pt. These two factors thus contribute to a similar extent to the different behavior of group 9 and group 10 metal complexes [M(SPS)(X)] toward the oxidative addition of H_2.

These results led us to search for H_2 addition products which kept unchanged the oxidation number of the metal center. Molecular dihydrogen complexes were actually optimized and characterized as minima for the two Pd complexes (**VIIc**,**d**) and for the Pt (**VIIe**) complex with X = Cl (Figure 8). In these structures, a sulfur center is decoordinated and a nearly square-planar arrangement is found at the Pd(II) or Pt(II) metal center.

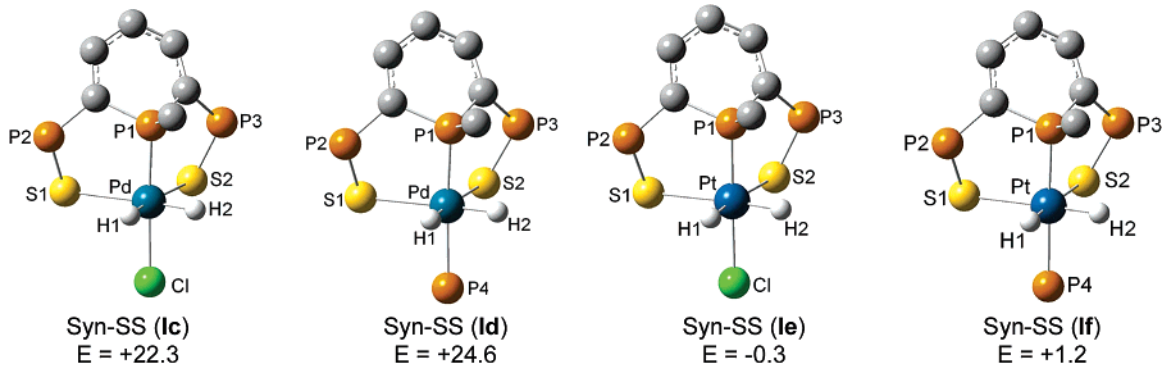

Figure 7. Optimized geometries of unsubstituted palladium and platinum complexes **Ic**−**f** (*syn*-SS isomers). Hydrogen atoms are omitted for clarity, except for those bound to the metal center. Selected geometrical parameters (bond distances in Å and angles in deg) are as follows. **Ic**: Pd−H1 = 1.521; S−Pd−S = 96.6, P1−Pd−Cl = 173.2. **Id**: Pd−H1 = 1.540; S−Pd−S = 97.0, P1−Pd−P4 = 172.3. **Ie**: Pd−H1 = 1.544; S−Pt−S = 94.2, P1−Pt−Cl = 177.5. **If**: Pt−H1 = 1.560; S−Pt−S = 93.8, P1−Pt−P4 = 176.1. *E*, given in kcal mol^{-1}, is the energy compared to that of the starting material.

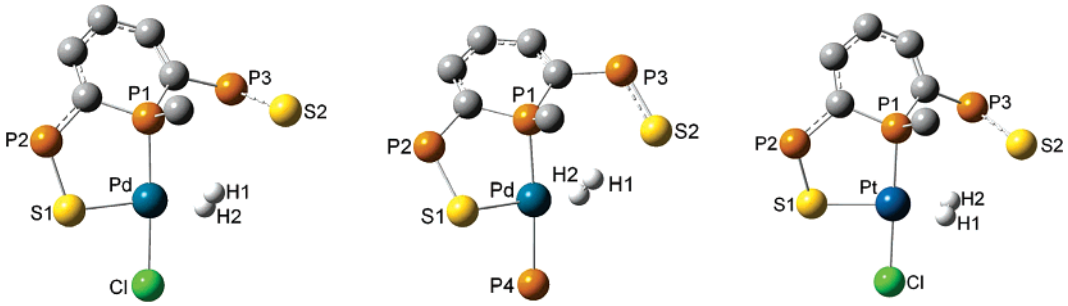

Figure 8. Optimized geometries of unsubstituted palladium and platinum molecular dihydrogen complexes **VIIc**−**e**. Hydrogen atoms are omitted for clarity, except for those bound to the metal center. Selected geometrical parameters (bond distances in Å and angles in deg) are as follows. **VIIc**: H1−H2 = 0.814, Pd−H1 = 1.792, Pd−S1 = 2.346, Pd−S2 = 4.493; S1−Pd−H1 = 168.7. **VIId**: H1−H2 = 0.834, Pd−H1 = 1.864, Pd−S1 = 2.406, Pd−S2 = 3.953; S1−Pd−H1 = 163.2. **VIIe**: H1−H2 = 0.931, Pd−H1 = 1.642, Pd−S1 = 2.355, Pd−S2 = 4.145; S1−Pd−H1 = 161.6. Energies are given in kcal mol^{-1} with respect to the starting materials.

Table 7. Energy Variation (ΔE_R, in kcal mol^{-1}) Associated with the Formation of the *syn*-SS Dihydride Complex I, the Molecular Dihydrogen Complex VII, and the Monohydride MH···SH Complex VI by Addition of H_2 on the Pd and Pt Starting Materials

	PdCl (**c**)	$PdPH_3^+$ (**d**)	PtCl (**e**)	$PtPH_3^+$ (**f**)
syn-SS (**I**)	+22.3	+24.6	−0.3	+1.2
Mol. H_2 (**VII**)	+11.7	+20.0	+8.1	
MH···SH (**VI**)	+9.0	+8.2	+1.9	+0.2

For the Pd compounds, these molecular dihydrogen complexes (**VIIc** and **VIId**) were found to be more stable than the corresponding *syn*-SS dihydride isomers (**Ic** and **Id**), by 10.6 and 4.6 kcal mol^{-1}, respectively. On the other hand, the Pt(IV) *syn*-SS dihydride (**Ie**) remains more stable than the Pt(II) molecular dihydrogen complex (**VIIe**) by 8.4 kcal mol^{-1} (Table 7).

Other minima with a M(II) metal center were found for the four starting complexes. They can be described as resulting from a heterolytic activation of H_2: a monohydride complex is formed by the addition of H^- on the metal, while H^+ adds to a lone pair of a decoordinated sulfur center (Figure 9).[14] These complexes, quoted as [MH···SH], were found to be the most stable addition product for the Pd complexes, located 9.0 and 8.2 kcal mol^{-1} above the reactants for X = Cl (**VIc**) and X = $(PH_3)^+$ (**VId**), respectively (Table 7). On the other hand, they turn out to be competitive with the *syn*-SS dihydride of the Pt complexes (**Ie**,**f**), the computed reaction energy ΔE_R being close to zero (+1.9 and +0.2 kcal mol^{-1} for **VIe**,**f**, respectively) (Table 6). Note, however, that the ΔG_R values associated with these [MH···SH] complexes are all positive (19.4, 17.5, 11.4, and 10.3 kcal mol^{-1} for **VIc**−**f**, respectively).

In conclusion, the oxidative addition of H_2 on group 10 [M(SPS)(X)] complexes (X = Cl, $(PH_3)^+$) leading to M(IV) dihydrides is found to be easier for Pt than for Pd complexes. For the latter, molecular dihydrogen and monohydride M(II) adducts are significantly more stable, while the monohydride complex is competitive in energy with the dihydride in the case of platinum. In marked contrast with the results obtained for group 9 metals, the energy variations ΔE_R associated with these addition reactions are either positive or close to zero and the associated ΔG_R values are always positive. These results are in agreement with the experimental observation, since no reaction occurs, even under high hydrogen pressure, between H_2 and group 10 d^8 [M(SPS)(X)] complexes.

Experimental Section

General Considerations. All reactions were routinely performed under an inert atmosphere of argon or nitrogen by using Schlenk and glovebox techniques and dry deoxygenated solvents. Dry THF and hexanes were obtained by distillation from Na/benzophenone. Dry ether was obtained by distillation from $CaCl_2$ and then NaH and dry CH_2Cl_2 from P_2O_5. CD_2Cl_2 and THF-d_8 were stored on 4 Å Linde molecular sieves in the glovebox. Nuclear magnetic resonance spectra were recorded on a Brüker Advance 300 spectrometer operating at 300.0 MHz for ^1H, 75.5 MHz for ^{13}C, and 121.5 MHz for ^{31}P. Solvent peaks are used as internal reference relative to Me_4Si for ^1H and ^{13}C chemical shifts (ppm); ^{31}P chemical shifts are relative to a 85% H_3PO_4 external reference. Coupling constants are given in hertz. The following abbreviations are used: s, singlet; d, doublet; t, triplet; q, quadruplet; p, pentuplet; m, multiplet; v, virtual. Elemental analyses were performed by the "Service d'analyse du CNRS", at Gif sur Yvette, France. Complexes **1**,[5] **2**,[6] and **5**[4] were prepared according to reported procedures.

Synthesis of Complex 3. H_2 (1 atm) was bubbled for 30 s into a freshly prepared solution of **1** in THF-d_8 (0.5 mL) at room temperature. The solution immediately turned from brown to deep orange. The lifetime of complex **3** was approximately several minutes in solution (THF) at room temperature under a N_2 atmosphere. Due to its intrinsic instability, complex **3** was only characterized by ^{31}P and ^1H NMR spectroscopy. ^{31}P NMR and ^1H NMR of the crude mixture revealed the formation of a single product. ^1H NMR (THF-d_8): δ −14.64 (dt, ^1J(H−Rh) = 24.5, ^2J(H−P_A) = ^2J(H−P_C) = 12.3, 2H, Rh−H), 1.83 (m, 3H, CH_3), 5.60 (vq, ^4J(H−P_B) = ^4J(H−P_A) = 3.7, 1H, H_4), 6.80−7.84 (m, 45H, H of Ph). ^{31}P NMR (THF-d_8; second-order spectrum which could not be modeled): δ 36.5−47.9 (AB_2C, m, P_AMe and P_C-PH_3), 49.6−50.8 (AB_2C, m, $\sum J$ = 145.8, P_BPh_2).

Synthesis of Complex 4. H_2 (1 atm) was bubbled for 3 min into a freshly prepared solution of **2** (C = 0.05 M, 0.15 mmol) in THF (3 mL) at room temperature. The solution immediately turned from brown to deep orange. After the solvent was removed, the solid was washed first with hexanes (3 × 2 mL) and then with diethyl ether (3 × 2 mL). The resulting solid was dissolved in CH_2-Cl_2 and the solution filtered through Celite. After drying, **4** was recovered as a yellow solid. Yield: 130 mg (76%). Anal. Calcd for $C_{60}H_{51}IrP_4S_2$ (1152.2): C, 62.54; H, 4.46. Found: C, 62.24; H, 4.17. ^1H NMR (CD_2Cl_2): δ −18.39 (vt, ^2J(H−P_A) = ^2J(H−P_Y) = 15.5), 1.87 (d, ^2J(H−P_A) = 8.7, 3H, CH_3), 5.60 (t, ^4J(H−P_B) = 5.6, 1H, H_4), 6.73−8.12 (m, 45H, H of Ph). ^{13}C NMR (CD_2Cl_2): δ 20.4 (m, CH_3), 71.4 (m, $C_{2,6}$), 116.4 (m, C_4H), 127.2−134.5 (m, CH and C of Ph), 137.4 (dd, J(H−P) = 44.6, J(H−P) = 4.0, C of Ph), 141.7 (bs, $C_{3,5}$), 154.2 (bs, C of Ph). ^{31}P NMR (CD_2-Cl_2): δ 9.7 (AB_2Y, td, ^2J(P_A−P_Y) = 336.0, ^2J(P_B−P_A) = 107.0,

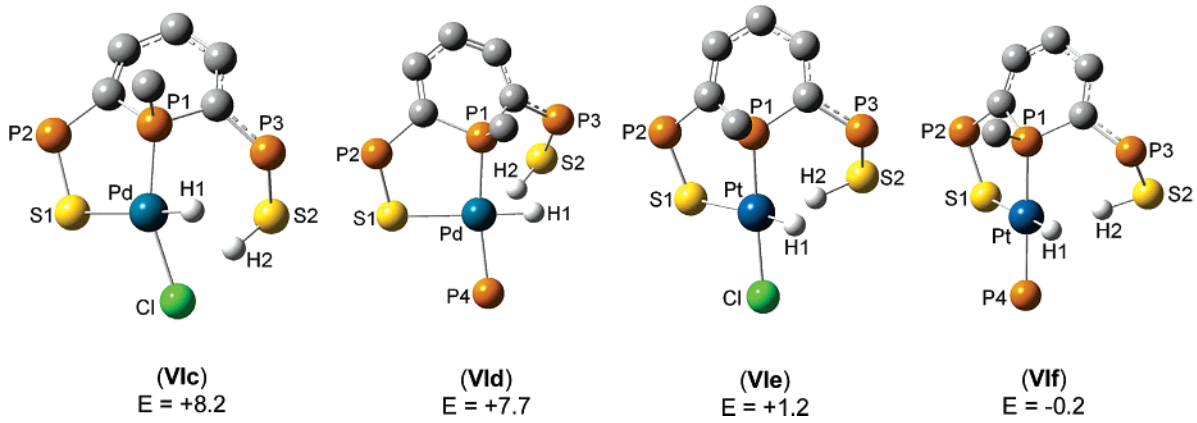

(VIc) E = +8.2 **(VId)** E = +7.7 **(VIe)** E = +1.2 **(VIf)** E = -0.2

Figure 9. Optimized geometries of unsubstituted palladium and platinum complexes **VIc**−**f**. Hydrogen atoms are omitted for clarity, except for those bound to the metal and to the decoordinated S centers. Selected geometrical parameters (bond distances in Å and angles in deg) are as follows. **VIc**: Pd−H1 = 1.535, Pd−S1 = 2.538, S2−H2 = 1.403, H2−Cl = 2.143; S1−Pd−H1 = 176.2, P1−Pd−Cl = 156.7. **VId**: Pd−H1 = 1.555, Pd−H2 = 2.745, Pd−S1 = 2.458, S2−H2 = 1.359; S1−Pd−H1 = 178.9. **VIe**: Pt−H1 = 1.553, Pt−H2 = 1.931, Pt−S1 = 2.520, S2−H2 = 1.491; S1−Pt−H1 = 175.5. **VIf**: Pt−H1 = 1.571, Pt−H2 = 2.265, Pt−S1 = 2.461, S2−H2 = 1.394; S1−Pt−H1 = 178.7. Energies (in kcal mol^{-1}) are given with respect to the starting materials.

P_AMe), 16.8 (dt, $^2J(P_Y-P_A)$ = 336.0, $^3J(P_Y-P_B)$ = 27.7, P_YPh_3), 50.3 (dd, $^2J(P_B-P_A)$ = 107.0, $^3J(P_B-P_Y)$ = 27.7, P_BPh_2).

Computational Details. Calculations were performed with the GAUSSIAN 03 series of programs.[18] Density functional theory (DFT)[19] was applied for the unsubstituted complexes (in which the phenyl substituents were replaced by H atoms) with the B3PW91 functional.[20] A quasi-relativistic effective core potential operator was used to represent the 28 innermost electrons of the rhodium and palladium atoms and the 60 innermost electrons of iridium and platinum atoms.[21] The basis set for the metal was that associated with the pseudopotential, with a standard double-ζ LANL2DZ contraction[21] completed by a set of polarization f functions.[22] Geometry optimizations on the model complexes were performed with the 6-31+G* basis for P, S, and Cl atoms, 6-31G* for the carbon atoms, 6-31++G** for the hydrogen atoms of H_2, and 6-31G for the other hydrogen atoms (basis set A).[23] The stationary points were characterized by full vibration frequency calculations. The energies were then recomputed using the same basis set on the metal center and the 6-31++G** basis set for all the other atoms (basis set B).[23] Note that the changes in relative energies were found to be lower than 1.0 kcal mol^{-1} on going from basis set A to basis set B. The ΔG values, given at 298 K, are derived from calculations with the basis set A, since they require the frequency calculations. QM/MM optimizations of real complexes were performed at the ONIOM(B3PW91:UFF) level with the phenyl substituents in the MM part.[24] The QM part was treated at the DFT-B3PW91 level with basis set A (see above), and the UFF force field was used for the MM part.[25] Finally, DFT-B3PW91 single-point calculations were performed on the optimized structures (B3PW91//B3PW91:UFF calculations) using the 6-31G basis set for the C and H atoms of the phenyl substituents and the basis set B for the other atoms.

X-ray Crystallographic Study. Crystals of compound **4** suitable for X-ray diffraction were obtained by slow evaporation of CD_2Cl_2. Data were collected at 150.0(1) K on a Nonius Kappa CCD diffractometer using a Mo Kα (λ = 0.710 70 Å) X-ray source and a graphite monochromator. All data were measured using ψ and ω scans. Experimental details are described in Table 1. The crystal structures were solved using SIR 97[26] and Shelxl-97.[27] ORTEP drawings were made using ORTEP III for Windows.[28] CCDC-286775 contains the supplementary crystallographic data for this paper. These data can be obtained free of charge at www.ccdc.cam.ac.uk/conts/retrieving.html (or from the Cambridge Crystallographic Data Centre, 12, Union Road, Cambridge CB2 1EZ, U.K.; fax (internat.) +44-1223/336-033; e-mail deposit@ccdc.cam.ac.uk.

Acknowledgment. We thank the CNRS, the DGA, and the École polytechnique for supporting this work. IDRIS (Project No. 061616) is also acknowledged for the allowance of computer time.

Supporting Information Available: Figures and tables giving the optimized geometry, energy, and frequencies of [M(SPS)(PR_3)] (M = Rh, Ir; R = PH_3, PPh_3), **Ia**−**VIa**, **Ib**−**VIb**, **Ia-rc**, **Ib-rc**,

(18) Frisch, M. J.; Trucks, G. W.; Schlegel, H. B.; Scuseria, G. E.; Robb, M. A.; Cheeseman, J. R.; Montgomery, J. A., Jr.; Vreven, T.; Kudin, K. N.; Burant, J. C.; Millam, J. M.; Iyengar, S. S.; Tomasi, J.; Barone, V.; Mennucci, B.; Cossi, M.; Scalmani, G.; Rega, N.; Petersson, G. A.; Nakatsuji, H.; Hada, M.; Ehara, M.; Toyota, K.; Fukuda, R.; Hasegawa, J.; Ishida, M.; Nakajima, T.; Honda, Y.; Kitao, O.; Nakai, H.; Klene, M.; Li, X.; Knox, J. E.; Hratchian, H. P.; Cross, J. B.; Bakken, V.; Adamo, C.; Jaramillo, J.; Gomperts, R.; Stratmann, R. E.; Yazyev, O.; Austin, A. J.; Cammi, R.; Pomelli, C.; Ochterski, J. W.; Ayala, P. Y.; Morokuma, K.; Voth, G. A.; Salvador, P.; Dannenberg, J. J.; Zakrzewski, V. G.; Dapprich, S.; Daniels, A. D.; Strain, M. C.; Farkas, O.; Malick, D. K.; Rabuck, A. D.; Raghavachari, K.; Foresman, J. B.; Ortiz, J. V.; Cui, Q.; Baboul, A. G.; Clifford, S.; Cioslowski, J.; Stefanov, B. B.; Liu, G.; Liashenko, A.; Piskorz, P.; Komaromi, I.; Martin, R. L.; Fox, D. J.; Keith, T.; Al-Laham, M. A.; Peng, C. Y.; Nanayakkara, A.; Challacombe, M.; Gill, P. M. W.; Johnson, B.; Chen, W.; Wong, M. W.; Gonzalez, C.; Pople, J. A. *Gaussian 03*, revision C.02; Gaussian, Inc.: Wallingford, CT, 2004.

(19) (a) Ziegler, T. *Chem. Rev.* **1991**, *91*, 651−667. (b) Parr, R. G.; Yang, W. *DFT*; Oxford University Press: Oxford, U.K., 1989.

(20) Becke, A. D. *J. Chem. Phys.* **1993**, *98*, 5648−5652.

(21) Hay, P. J.; Wadt, W. R. *J. Chem. Phys.* **1985**, *82*, 299−310.

(22) Ehlers, A.; Böhme, M.; Dapprich, S.; Gobbi, A.; Höllwarth, A.; Jonas, V.; Köhler, K. F.; Stegmann, R.; Veldkamp, A.; Frenking, G. *Chem. Phys. Lett.* **1993**, *208*, 111−114.

(23) (a) Clark, T.; Chandrasekhar, J.; Spitznagel, G. W.; Schleyer, P. v. R. *J. Comput. Chem.* **1983**, *4*, 294−301. (b) Francl, M. M.; Pietro, W. J.; Hehre, W. J.; Binkley, J. S.; Gordon, M. S.; DeFrees, D. J.; Pople, J. A. *J. Chem. Phys.* **1982**, *77*, 3654−3665. (c) Hehre, W. J.; Ditchfield, R.; Pople, J. A. *J. Chem. Phys.* **1972**, *56*, 2257−2272. (d) Hariharan, P. C.; Pople, J. A. *Theor. Chim. Acta* **1973**, *28*, 213−222.

(24) Svensson, M.; Humbel, S.; Froese, R. D. J.; Matsubara, T.; Sieber, S.; Morokuma, K. J. *J. Phys. Chem.* **1996**, *100*, 19357−19363.

(25) Rappé, A. K.; Casewitt, C. J.; Colwell, K. S.; Goddard, W. A.; Skiff, W. M. *J. Am. Chem. Soc.* **1992**, *114*, 10024−10035.

(26) Altomare, A.; Burla, M. C.; Camalli, M.; Cascarano, G.; Giacovazzo, C.; Guagliardi, A.; Moliterni, A. G. G.; Polidori, G.; Spagna, R. *SIR97*, an integrated package of computer programs for the solution and refinement of crystal structures using single-crystal data.

(27) Sheldrick, G. M. *SHELXL-97*; Universität Göttingen, Göttingen, Germany, 1997.

(28) Farrugia, L. J. *ORTEP-3*; Department of Chemistry, University of Glasgow, Glasgow, Scotland.

TS-Ia, **TS-Ib**, [M(SPS)(X)] (M = Pd, Pt, X= Cl, PH_3^+), **Ic**−**f**, **VIc**−**f**, and **VIIc**−**e**, the entropy and free energy for [M(SPS)-(PH_3)] (M = Rh, Ir), **Ia**−**b, TS-Ia**, and **TS-Ib**, and crystal data for **4**. This material is available free of charge via the Internet at http://pubs.acs.org.

OM050900U